European Journal of Pharmaceutics and Biopharmaceutics 203 (2024) 114476

Contents lists available at ScienceDirect

European Journal of Pharmaceutics and Biopharmaceutics

journal homepage: www.elsevier.com/locate/ejpb

Development of dual-crosslinked Pluronic F127/Chitosan injectable hydrogels incorporating graphene nanosystems for breast cancer photothermal therapy and antibacterial applications

Manuel R. Pouso [a], Bruna L. Melo [a,b], Joaquim J. Gonçalves [a,b], António G. Mendonça [a,c], Ilídio J. Correia [a,b,d,*], Duarte de Melo-Diogo [a,*]

[a] CICS-UBI – Centro de Investigação Em Ciências Da Saúde, Universidade Da Beira Interior, Covilhã, Portugal
[b] AEROG-LAETA, Aerospace Sciences Department, Universidade Da Beira Interior, Covilhã, Portugal
[c] Departamento de Química, Universidade Da Beira Interior, 6201-001 Covilhã, Portugal
[d] University of Coimbra, CERES, Department of Chemical Engineering, 3030-790 Coimbra, Portugal

ARTICLE INFO

Keywords:
Antimicrobial applications
Cancer therapy
Chitosan hydrogels
Injectable hydrogels
Photothermal therapy
Pluronic F127 hydrogels
Reduced graphene oxide

ABSTRACT

Nanomaterials with responsiveness to near-infrared light can mediate the photoablation of cancer cells with an exceptional spatio-temporal resolution. However, the therapeutic outcome of this modality is limited by the nanostructures' poor tumor uptake. To address this bottleneck, it is appealing to develop injectable *in situ* forming hydrogels due to their capacity to perform a tumor-confined delivery of the nanomaterials with minimal off-target leakage. In particular, injectable *in situ* forming hydrogels based on Pluronic F127 have been emerging due to their FDA-approval status, biocompatibility, and thermosensitive sol–gel transition. Nevertheless, the application of Pluronic F127 hydrogels has been limited due to their fast dissociation in aqueous media. Such limitation may be addressed by combining the thermoresponsive sol–gel transition of Pluronic F127 with other polymers with crosslinking capabilities. In this work, a novel dual-crosslinked injectable *in situ* forming hydrogel based on Pluronic F127 (thermosensitive gelation) and Chitosan (ionotropic gelation in the presence of $NaHCO_3$), loaded with Dopamine-reduced graphene oxide (DOPA-rGO; photothermal nanoagent), was developed for application in breast cancer photothermal therapy. The dual-crosslinked hydrogel incorporating DOPA-rGO showed a good injectability (through 21 G needles), *in situ* gelation capacity and cytocompatibility (viability > 73 %). As importantly, the dual-crosslinking improved the hydrogel's porosity and prevented its premature degradation. After irradiation with near-infrared light, the dual-crosslinked hydrogel incorporating DOPA-rGO produced a photothermal heating ($\Delta T \approx 22$ °C) that reduced the breast cancer cells' viability to just 32 %. In addition, this formulation also demonstrated a good antibacterial activity by reducing the viability of *S. aureus* and *E. coli* to 24 and 33 %, respectively. Overall, the dual-crosslinked hydrogel incorporating DOPA-rGO is a promising macroscale technology for breast cancer photothermal therapy and antimicrobial applications.

1. Introduction

Over the years, there has been a rise in the development of nanomaterials aimed for anticancer applications [1,2]. This growth has been driven by the ability of the nanostructures to encapsulate chemotherapeutic drugs (*e.g.*, doxorubicin, paclitaxel, cisplatin, 5-fluorouracil) [3–5], thus enhancing their solubility [1,6,7]. Another driving force is correlated with the capability of nanomaterials to accumulate at the tumor zone, through the *so-called* Enhanced Permeability and Retention (EPR) effect, thereby improving the safety of the

Abbreviations: ANOVA, Analysis of variance; DMEM-F12, Dulbecco's Modified Eagle's Medium F-12; DOPA-rGO, Dopamine-reduced Graphene Oxide; DOPA-rGO@PC-gel, Pluronic F127/Chitosan injectable *in situ* forming hydrogel loaded with DOPA-rGO; *E. coli*, *Escherichia coli*; EPR, Enhanced Permeability and Retention; FBS, Fetal Bovine Serum; MCF-7, Michigan Cancer Foundation-7; NHDF, Normal Human Dermal Fibroblasts; NIR, Near-Infrared; n.s., non-significant; PBS, Phosphate Buffered Saline; PC-gel, Pluronic F127/Chitosan injectable *in situ* forming hydrogel; P-gel, Pluronic F127 injectable *in situ* forming hydrogel; *S. aureus*, *Staphylococcus aureus*; S.D., Standard Deviation; SEM, Scanning Electron Microscopy.

* Corresponding authors.
E-mail addresses: icorreia@ubi.pt (I.J. Correia), demelodiogo@fcsaude.ubi.pt (D. de Melo-Diogo).

https://doi.org/10.1016/j.ejpb.2024.114476
Received 17 July 2024; Received in revised form 23 August 2024; Accepted 25 August 2024
Available online 28 August 2024

treatments [7,8]. However, the therapeutic efficacy of the drug-loaded nanomaterials has been severely limited by the drug-resistance mechanisms developed by cancer cells (*e.g.*, overexpression of drug efflux pumps, upregulation of repair machinery) [9,10].

To address this challenge, researchers have started to engineer nanomaterials with capacity to induce damage to the cancer cells through alternative pathways. In this regard, nanomaterials with responsiveness to Near-Infrared (NIR; 750 – 1000 nm) light have been showing excellent results for cancer therapy [11]. After reaching the tumor, these nanomaterials can absorb and convert NIR light into heat (a process known as photothermal therapy) [11]. The photoinduced heat generated by the nanomaterials may then induce irreversible damages to the cancer cells (*e.g.,* protein denaturation, lipid melting), leading to their death when the local temperature exceeds 50 °C [12–14]. In cancer photothermal therapy, the use of NIR light is essential due to its minimal interactions with biological components (*e.g.*, water, melanin, hemoglobin), ensuring that the nanostructures' photothermal effect has a good spatio-temporal resolution [12]. For instance, Chen's team reported that poly(ethylene glycol)-functionalized gold bellflowers could produce a localized photothermal heating to ≈ 54 °C, being this hyperthermic effect responsible for *in vivo* tumor eradication [14]. Zheng's team reported that poly(vinylpyrrolidone)-coated poly(pyrrole) nanoparticles could generate a localized photoinduced heating to ≈ 65 °C that caused the elimination of mice's tumors [15].

Despite the exciting results reported in *in vitro* and *in vivo* studies, the translation of the nanomaterials into the clinic has been limited by their weak tumor accumulation [16]. In fact, Chan's group showed that less than 1 % (median) of the intravenously administered nanomaterials reach the tumor [17]. After systemic administration (*i.e.*, intravenous injection), the nanomaterials can undergo opsonization, leading to their clearance by the reticuloendothelial system [18,19]. Moreover, the intravenously administered nanomaterials depend heavily on the EPR effect to reach the tumor site [20]. However, the EPR effect has been found to be overexaggerated in preclinical cancer models and it is not present in all human tumors [20,21].

The challenges associated with the systemic administration of the nanomaterials have motivated the development of technologies capable of performing the local delivery of the nanomaterials into the tumor site [22,23]. In this regard, the use of injectable *in situ* forming hydrogels is emerging owed to their straightforward preparation and ability to perform a tumor-confined delivery of the therapeutics with minimal off-target leakage [24–26]. In this approach, the hydrogel's precursor solution (*e.g.*, polymers, crosslinkers) is mixed with the nanomaterials, being then intratumorally injected [22]. Afterwards, this solution achieves *in situ* gelation by physical and/or chemical interactions, leading to the assembly of the nanoparticle-loaded hydrogel [22,27]. Indeed, the application of injectable hydrogels to perform the local delivery of the nanomaterials can greatly outperform the standalone administration of the nanoparticles [28,29]. In this regard, Kong's team compared the biodistribution of intravenously (systemic) administered nanoparticles with that achieved using an injectable hydrogel to perform their local delivery [28]. In this case, the tumor accumulation of the nanoparticles was ≈ 8.0-times higher when locally delivered by the injectable hydrogel [28]. The systemically administered nanoparticles had a lower tumor uptake and greater accumulation in the off-target organs (kidneys, liver, lungs) [28]. Qian's team reported that the local delivery of nanomaterials using injectable hydrogels could achieve a ≈ 5.2-times higher tumor uptake when compared to the direct administration of the nanoparticles [29]. As importantly, these injectable hydrogels can sustain the delivery of the nanoparticles into the tumor for up to 14 days, while the sole use of the nanoparticles resulted in a rapid clearance within 1–3 days [29].

Recently, injectable *in situ* forming hydrogels based on Pluronic F127 (*i.e.*, poly(ethylene oxide)-poly(propylene oxide)-poly(ethylene oxide)) have started to gather significant interest for local delivery applications due to their FDA-approval status (as excipient), biocompatibility and thermosensitive sol–gel transition [30,31]. The Pluronic F127 is liquid at low temperatures (*e.g.*, 4 °C) but it can transition into a hydrogel at physiological temperatures (37 °C) [31]. Despite these advantages, the application of Pluronic F127-based hydrogels has been limited by their fast dissociation in aqueous media [32,33]. In fact, Pluronic F127-based hydrogels can become completely disintegrated (100 % degradation) in just 1 day of immersion in aqueous environments [32], compromising their capacity to sustain the delivery of the therapeutics. Therefore, combining the thermoresponsive sol–gel transition of Pluronic F127 with other polymers/materials with crosslinking capabilities could be a promising approach to overcome the previous limitation [32,34]. Additionally, the incorporation other polymers/materials into the Pluronic F127 hydrogels may introduce new functionalities (*e.g.*, antimicrobial properties), further enhancing the hydrogels' therapeutic potential. To the best of our knowledge, multi-crosslinked Pluronic F127-based injectable hydrogels designed for cancer photothermal therapy have not yet been developed.

In this work, and for the first time, a dual-crosslinked Pluronic F127-based injectable *in situ* forming hydrogel incorporating Dopamine-reduced graphene oxide (DOPA-rGO) was prepared for application in cancer photothermal therapy. This novel DOPA-rGO loaded dual-crosslinked injectable hydrogel was assembled by combining Pluronic F127 (thermosensitive gelation) with Chitosan (ionotropic gelation in the presence of $NaHCO_3$). Besides its ionotropic gelation capacity, Chitosan was also selected due to its biocompatibility and antibacterial properties towards gram-positive and gram-negative bacteria [35]. In turn, DOPA-rGO was chosen as the photothermal nanoagent since our research group has previously demonstrated its high photothermal capacity under NIR laser irradiation (808 nm, 1.7 W/cm^2) [36]. As importantly, the DOPA-rGO produced by our team presented an excellent cytocompatibility profile, even at high doses (100 μg/mL) [36].

The obtained data revealed that the produced dual-crosslinked hydrogel incorporating DOPA-rGO has a good injectability (through 21 G needles), *in situ* gelation capacity and cytocompatibility (viability > 73 %). As importantly, the dual-crosslinking improved the hydrogel's porosity and prevented its premature degradation. After irradiation with NIR light, the dual-crosslinked hydrogel incorporating DOPA-rGO produced a photothermal heating (ΔT ≈ 22 °C) that reduced the viability of the breast cancer cells to just 32 %. In addition, this formulation also demonstrated a good antibacterial activity by reducing the viability of *S. aureus* and *E. coli* to 24 and 33 %, respectively.

2. Materials and methods

2.1. Materials

Pluronic F127, Chitosan (low molecular weight), Graphene Oxide nanocolloids, Dulbecco's modified Eagle's medium F-12 (DMEM-F12), penicillin/streptomycin/amphotericin B, trypsin, Phosphate buffered saline (PBS), LB Broth and resazurin were obtained from Sigma Aldrich (Sintra, Portugal). $NaHCO_3$ was acquired from Fisher Scientific (Oeiras, Portugal). Dopamine hydrochloride was obtained from Acros Organics (New Jersey, USA). Lysozyme from chicken egg was obtained from Alfa Aesar (Haverhill, MA, USA). Fetal bovine serum (FBS) was bought from Biochrom AG (Berlin, Germany). Michigan cancer foundation-7 (MCF-7) cell line was obtained from ATCC (Middlesex, UK). Normal human dermal fibroblasts (NHDF) were acquired from PromoCell (Heidelberg, Germany). *Staphylococcus aureus* clinical isolate (*S. aureus*; ATCC 25923) and *Escherichia coli* DH5a (*E. coli*) were used to evaluate the antimicrobial properties. Cell culture plates and T-flasks were purchased from Thermo Fisher Scientific (Porto, Portugal). Water used in all experiments was double deionized (0.22 μm filtered, 18.2 MΩ cm).

2.2. Methods

2.2.1. Production of the dual-crosslinked Pluronic F127/Chitosan injectable in situ forming hydrogel loaded with DOPA-rGO

The dual-crosslinked thermosensitive injectable *in situ* forming hydrogel loaded with DOPA-rGO was prepared by adapting a protocol described in a previous study [34]. The DOPA-rGO was produced following the method previously described by our team [36], being its synthesis and characterization reported in the Supplementary Information.

Initially, a solution containing Pluronic F127 (20 % (w/v)) and Chitosan (3.33 % (w/v)) was prepared (solvent HCl (0.1 M)) in an ice-cold bath. Afterwards, this Pluronic F127/Chitosan solution (156 μL) was mixed with the DOPA-rGO (56.4 μL; 886 μg/mL) and $NaHCO_3$ (37.6 μL; 22.6 mg/mL; dissolved in PBS) solutions. The resulting Pluronic F127/Chitosan/$NaHCO_3$/DOPA-rGO solution was then loaded into a syringe equipped with a 21 G needle (0.8 x 25 mm), and it was extruded, originating the dual-crosslinked Pluronic F127/Chitosan injectable *in situ* forming hydrogel loaded with DOPA-rGO (abbreviated as DOPA-rGO@PC-gel). To create hydrogels with similar macroscopic properties for the different assays, the Pluronic F127/Chitosan/$NaHCO_3$/DOPA-rGO solution (250 μL) was also extruded into removable hollow cylindrical templates (ϕ = 9 mm; height = 4 mm). As controls, hydrogels were also prepared using only Pluronic F127/Chitosan/$NaHCO_3$ (abbreviated as PC-gel) and using only Pluronic F127 (abbreviated as P-gel), following the procedures described above.

2.2.2. Characterization of the hydrogels

The gelation of the DOPA-rGO@PC-gel, PC-gel and P-gel was assessed by using the inverted microtube test [37]. For such, the hydrogels' precursor materials (at 4 °C) were loaded into microtubes. The microtubes were left at room temperature and then, these were inverted to observe the gelation. The hydrogels' precursor materials were also extruded through syringes equipped with 21 G needles (0.8 × 25 mm), allowing the assessment of their injectability and *in situ* gelation [37]. The cross-sectional morphology of the DOPA-rGO@PC-gel, PC-gel and P-gel was analyzed by Scanning Electron Microscopy (SEM; Hitachi S-3400 N scanning electron microscope (Japan); acceleration voltage of 20 kV) [35]. The degradation profile of the DOPA-rGO@PC-gel, PC-gel and P-gel was assessed by incubating each formulation with a PBS solution (pH 7.4; 10 mL) containing Lysozyme (13.6 mg/L), for 7 days, under stirring, at 37 °C [35]. Then, the hydrogels were recovered (at each timepoint), rinsed with water, freeze-dried (ScanVac CoolSafe, LaboGene ApS, Lynge, Denmark), and weighted. The weight loss of the hydrogels (at each timepoint) was calculated according to the equation described below (W_i – hydrogel initial weight; W_t – hydrogel weight at time t).

$$Weight\ loss\ (\%) = \left(\frac{Wi - Wt}{Wi}\right) x\,100$$

The photothermal capacity of the DOPA-rGO@PC-gel and PC-gel was evaluated following a method previously described by our team [35]. For such, the hydrogels were immersed in water and then, these were exposed to NIR radiation (808 nm, 1.7 W/cm^2) for 10 min. The temperature changes (at each timepoint) were recorded using a thermocouple thermometer. Water irradiated with NIR light was used as the control. By last, the long-term storage stability of the DOPA-rGO@PC-gel's precursor solutions was investigated [37]. For this purpose, the Pluronic F127/Chitosan, $NaHCO_3$, and DOPA-rGO solutions were stored for 50 days. Afterwards, the stored solutions were mixed, loaded into a syringe, and extruded to evaluate the injectability and *in situ* gelation of the resulting DOPA-rGO@PC-gel.

2.2.3. Evaluation of the cytocompatibility of the DOPA-rGO@PC-gel

The cytocompatibility profile of the DOPA-rGO@PC-gel was evaluated on NHDF (healthy cell model) and MCF-7 cells (breast cancer cell model) using the resazurin method [38]. Both cell lines were cultured in DMEM-F12 medium supplemented with 10 % (v/v) of FBS and 1 % (v/v) of penicillin/streptomycin, in a humified incubator at 37 °C with 5 % of CO_2. For the cytocompatibility assay, the cells were harvested and seeded into 24-well plates at a density of 2.5 × 10^4 cells/well. After 48 h of growth, the cells were incubated with fresh culture medium along with the DOPA-rGO@PC-gel for 24 and 48 h. Afterwards, the DOPA-rGO@PC-gel was removed, and the cells were incubated with fresh culture medium containing resazurin (10 % (v/v)) for 4 h in the dark (37 °C, 5 % CO_2). The cells' viability was determined by analyzing the fluorescence of resorufin ($\lambda_{ex}/\lambda_{em}$ = 560/590 nm; Spectramax Gemini EM spectrofluorometer (Molecular Devices LLC, California, USA)). The cells incubated only with culture medium were used as the negative control (K-). The cells incubated with ethanol (70 % (v/v)) were used as the positive control (K+).

2.2.4. Evaluation of the phototherapeutic capacity of the DOPA-rGO@PC-gel

The phototherapeutic capacity of the DOPA-rGO@PC-gel was evaluated by using a method previously described by our team [38]. For this assay, the MCF-7 cells were seeded into 24-well plates as described in the section 2.2.3. After 48 h of growth, the culture medium was renewed, and the cells were incubated with the DOPA-rGO@PC-gel. Then, after 4 h of incubation, the hydrogels were exposed to NIR radiation (808 nm, 1.7 W/cm^2, 10 min). After reaching a total of 24 h of incubation with the hydrogels, the viability of the cells was quantified using the resazurin method (as described in section 2.2.3.).

2.2.5. Determination of the antibacterial activity of the DOPA-rGO@PC-gel

The antibacterial activity of the DOPA-rGO@PC-gel was assessed on gram-positive bacteria (*S. aureus*) and gram-negative bacteria (*E. coli*) [39]. The hydrogels (50 μL) were placed into 96-well plates along with bacterial suspensions (1 × 10^8 CFU/mL; in culture medium (LB Broth)). After 24 h, the medium was collected, and it was added with resazurin. After 4 h of incubation with resazurin, the viability of the bacteria was determined by measuring the fluorescence of resorufin ($\lambda_{ex}/\lambda_{em}$ = 545/590 nm). Bacteria only exposed to culture medium were used as the negative control (K-). Bacteria exposed to antibiotics (solution composed of penicilin, streptomycin and amphotericin B) were used as the positive control (K+).

2.2.6. Statistical analysis

Comparison between multiple groups was conducted by using the one-way Analysis of Variance (ANOVA) with the Student-Newman-Keuls test (a *p*-value lower than 0.05 ($p < 0.05$) was considered statistically significant). Data analysis was performed in GraphPad Prism v6.0 (Trial version, GraphPad Software, CA, USA).

3. Results and Discussion

3.1. Production and characterization of the DOPA-rGO@PC-gel

In order to assemble an injectable *in situ* forming hydrogel for cancer photothermal therapy, DOPA-rGO (photothermal nanoagent) was loaded into dual-crosslinked hydrogels composed of Pluronic F127 (thermosensitive gelation) and Chitosan (ionotropic gelation in the presence of $NaHCO_3$) – termed as DOPA-rGO@PC-gel (Fig. 1A).

The synthesized DOPA-rGO exhibited a nanometric size distribution (Figure S1A) and a high NIR absorption (Figure S1B). For comparison purposes, a hydrogel composed of Pluronic F127, Chitosan and $NaHCO_3$ (*i.e.*, without DOPA-rGO) was also prepared (termed as PC-gel).

A hydrogel formulated with only Pluronic F127 was also used as control (termed as P-gel).

The preparation of DOPA-rGO@PC-gel was a straightforward process, that only required the simple mixture of the Pluronic F127/

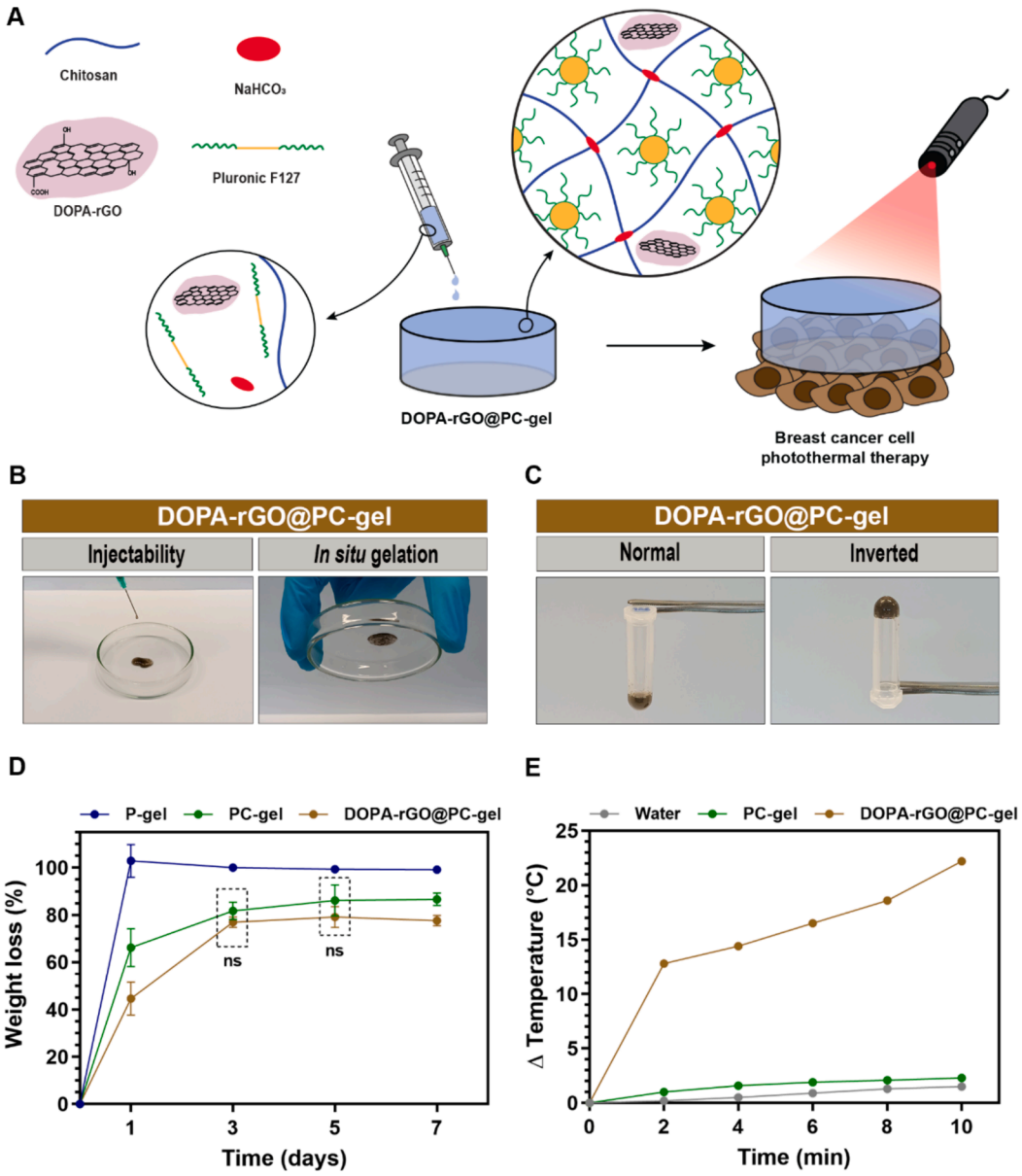

Fig. 1. Characterization of the physicochemical properties of P-gel, PC-gel and DOPA-rGO@PC-gel. Schematic illustration of the DOPA-rGO@PC-gel's assembly and application in the photothermal therapy of breast cancer cells (A). Macroscopic images of the injectability and *in situ* gelation of the DOPA-rGO@PC-gel (B). Macroscopic images of the DOPA-rGO@PC-gel's gelation, confirmed by the inverted microtube test (C). Evaluation of the hydrogels' weight loss during 7 days (D). Data presented as mean ± S.D., n = 5 (ns = non-significant). If the comparisons between the groups of the same incubation time were not identified, these were statistically significant ($p < 0.05$). Temperature variation curves of PC-gel, DOPA-rGO@PC-gel (99.94 μg/mL of DOPA-rGO) and water upon irradiation with NIR light (808 nm, 1.7 W/cm^2) during 10 min (E).

Chitosan solution with the $NaHCO_3$ and DOPA-rGO solutions. Then, this mixture was loaded into a syringe, and upon extrusion, the DOPA-rGO@PC-gel became assembled *in situ* (Fig. 1B). The gelation of the DOPA-rGO@PC-gel was also confirmed using the inverted microtube test (Fig. 1C). The DOPA-rGO@PC-gel's injectability and *in situ* gelation suggest that this formulation may be administered through a minimally invasive route, hence dismissing the need for a surgical incision to implant the hydrogel at the tumor site [22]. Similarly, the control hydrogels (PC-gel and P-gel) also exhibited injectability and *in situ* gelation (Figure S2 and S3).

The hydrogels' precursor solutions were also inserted into removable hollow cylindrical molds, allowing the assembly of three-dimensional structures with consistent macroscopic features for the remaining assays (Figure S4A). The SEM analysis revealed that both DOPA-rGO@PC-gel and PC-gel exhibited a well-defined and porous interconnected inner structure (Figure S4B). In contrast, the P-gel presented a compact inner structure without macropores (Figure S4B). In this way, the dual-crosslinking present in both DOPA-rGO@PC-gel and PC-gel contributed to the assembly of structures with interconnected pores, which is essential for the effective diffusion of the therapeutic compounds into the target site [40].

Afterwards, the degradation of the hydrogels in biologically mimicking fluids was evaluated. Following 1 day of incubation, the DOPA-rGO@PC-gel and the PC-gel experienced a degradation of 45 % and 63 %, respectively (Fig. 1D). By the 7th day of incubation, the DOPA-rGO@PC-gel and the PC-gel showed a degradation of 78 and 87 %, respectively (Fig. 1D). In contrast, the P-gel did completely disintegrate after just 1 day of incubation (100 % degradation; Fig. 1D). The premature degradation of the P-gel is in accordance with the behavior of other hydrogels derived from Pluronic F127 [32,33]. In this way, the

presence of the dual-crosslinking on both DOPA-rGO@PC-gel and PC-gel could effectively slow the hydrogels' degradation. Such is crucial since hydrogels with a premature degradation may release their cargo in a burst-manner, compromising the therapeutic response [41,42]. Notably, the presence of DOPA-rGO in the DOPA-rGO@PC-gel reduced even further the hydrogel's degradation. Such phenomenon may be attributed to the ability of graphene-derivatives to interact with different types of polymers (due to their large surface area), thus enhancing the stability of the hydrogels [32,35]. Based on these results, the DOPA-rGO@PC-gel and the PC-gel were selected for the subsequent assays.

Subsequently, it was evaluated the photothermal capacity of the DOPA-rGO@PC-gel and the PC-gel. For this purpose, the hydrogels were irradiated with NIR light (808 nm, 1.7 W/cm^2) for 10 min (Fig. 1E), and the temperature changes were recorded. The DOPA-rGO@PC-gel could generate a temperature increase of ≈ 22 °C (ΔT) after interacting with NIR light (Fig. 1E). This photothermal effect can potentially induce irreversible damages to the cancer cells, leading to their death [12]. The photothermal capacity of the DOPA-rGO@PC-gel is derived from the presence of DOPA-rGO in this formulation. In fact, NIR-absorbing nanomaterials can be loaded into hydrogels for attaining macroscale systems with an excellent photothermal capacity [38,43,44]. As expected, both PC-gel and water (control) showed minimal temperature increases (ΔT < 2 °C) when exposed to NIR light. The marginal photo-induced heat produced by water is consistent with the water's weak absorption at the wavelength of 808 nm, being in agreement with several literature reports [45,46]. The minimal temperature variation produced by the PC-gel upon NIR laser exposure can be justified by the fact this formulation does not have any high NIR-absorbing materials in its composition. In another study, Shen's team developed a chitosan-based hydrogel containing zinc oxide-graphene oxide nanohybrids, which produced a temperature increase of ≈ 22 °C (ΔT) after exposure to NIR light (250 μg/mL of hybrids; 808 nm, 2.0 W/cm^2, 6 min) [47]. In this work, the DOPA-rGO@PC-gel could produce a similar photothermal heating (ΔT ≈ 22 °C) at a considerably lower concentration and laser intensity (99.94 μg/mL of DOPA-rGO; 1.7 W/cm^2), but it required a slightly longer irradiation time (10 min). These results further confirm the good photothermal capacity of the DOPA-rGO@PC-gel, and thus this formulation was selected for the remaining assays.

Finally, the DOPA-rGO@PC-gel's precursor solutions were stored for an extended period of time (50 days) to assess whether these would still be able to promote the hydrogel's assembly. Upon mixture of the stored solutions (Pluronic F127/Chitosan, $NaHCO_3$, and DOPA-rGO), the resulting formulation continued to exhibit an excellent injectability and a thermoresponsive *in situ* gelation (Figure S5). This data highlights the good long-term storage stability of the hydrogel's precursor solutions, which is important for the future translation of the DOPA-rGO@PC-gel.

3.2. Evaluation of the cytocompatibility of the DOPA-rGO@PC-gel

After confirming the enhanced stability and photothermal capacity of the DOPA-rGO@PC-gel, the cytocompatibility of this formulation was evaluated on NHDF (healthy cells) and MCF-7 cells (breast cancer cells) – Fig. 2A.

The NHDF incubated with the DOPA-rGO@PC-gel for 24 and 48 h exhibited viabilities of 79 % and 73 %, respectively (Fig. 2B). Similarly, the MCF-7 cells exhibited viabilities of 77 % and 73 % after 24 and 48 h of incubation with the DOPA-rGO@PC-gel, respectively (Fig. 2C). These results indicate that the DOPA-rGO@PC-gel has an adequate cytocompatibility profile, being in agreement with the good biocompatibility of hydrogels formulated with Pluronic F127 and/or Chitosan [34,48,49]. For instance, Zang's team reported that synovial cells incubated with a Pluronic F127-based hydrogel for 48 h presented a viability of approximately 80 % [48]. In another work, Sabino *et al.* reported that NHDF and MCF-7 cells exposed to a Chitosan-based hydrogel for 48 h had a viability of about 90 % [49]. García-Couce *et al.* developed a hydrogel composed of Pluronic F127, Chitosan and Tripolyphosphate, demonstrating the cytocompatibility of this formulation towards C28/I2 cells (viability of about 84 % after 48 h of incubation) [34]. Additionally, our team has also previously reported the good safety profile of the DOPA-rGO [36]. Collectively, these findings support the cytocompatibility of the DOPA-rGO@PC-gel, thus allowing its use in cancer phototherapy (section 3.3.).

3.3. Evaluation of the photothermal therapy mediated by the DOPA-rGO@PC-gel

After confirming the adequate cytocompatibility profile of the DOPA-rGO@PC-gel, the phototherapeutic potential of this formulation towards breast cancer cells was investigated (Fig. 3A). For this purpose, the MCF-7 cells were initially incubated with the DOPA-rGO@PC-gel (99.94 μg/mL of DOPA-rGO), and then, the hydrogel was irradiated with NIR light (808 nm, 1.7 W/cm^2, 10 min).

Predictably, there were no changes observed in the viability of the MCF-7 cells only exposed to NIR light (Fig. 3B). Such finding is in agreement with the minimal photothermal heating caused by the NIR light *per se* (ΔT < 2 °C; Fig. 1E), and it is a consequence of the reduced

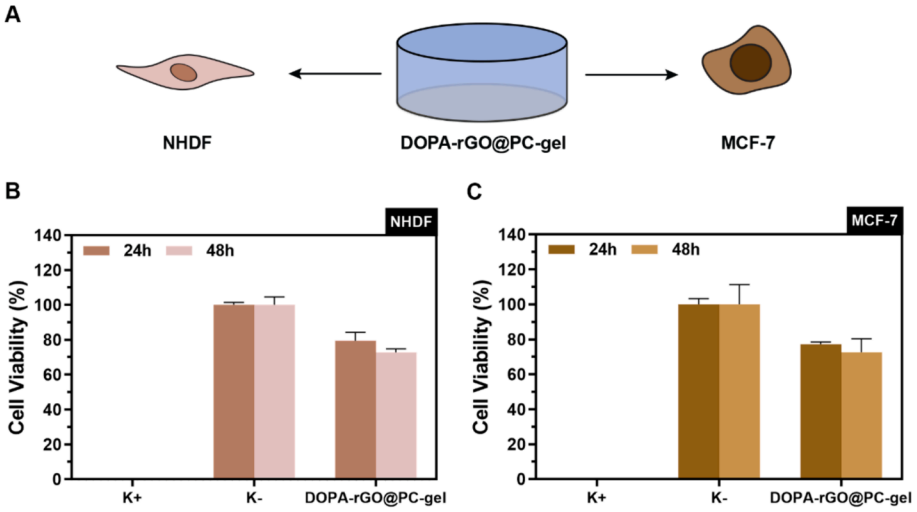

Fig. 2. Assessment of the cytocompatibility of the DOPA-rGO@PC-gel. Schematic illustration of the cytocompatibility assay (A). Viability of NHDF (B) and MCF-7 cells (C) after being exposed to the DOPA-rGO@PC-gel (99.94 μg/mL of DOPA-rGO) during 24 and 48 h. Data represents mean ± SD, n = 5. K- and K+ represent negative and positive controls, respectively.

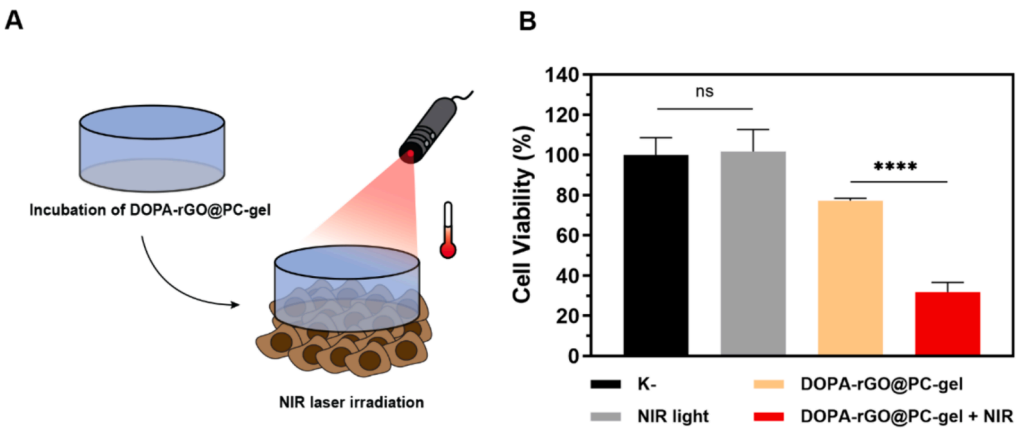

Fig. 3. Evaluation of the phototherapeutic effect mediated by the DOPA-rGO@PC-gel. Schematic illustration of the photothermal therapy mediated by the DOPA-rGO@PC-gel (A). Effect of the DOPA-rGO@PC-gel (99.94 μg/mL of DOPA-rGO) towards MCF-7 cells without NIR and with NIR laser irradiation (+NIR; 808 nm, 1.7 W cm^2, 10 min) (B). K- denotes the negative control and NIR light denotes the cells only exposed to the NIR laser irradiation (808 nm, 1.7 W cm^2, 10 min). Data represents mean ± S.D., n = 5 (**** $p < 0.0001$; n.s. = non-significant). The complete statistical analysis of the dataset of the Fig. 3B is reported in the Supplementary Information.

ability of the NIR light to interact with biological components [45,46]. Similarly, the non-irradiated DOPA-rGO@PC-gel did not affect meaningfully the MCF-7 cells (viability ≈ 77 %) – Fig. 3B. On the other hand, when the MCF-7 cells were exposed to DOPA-rGO@PC-gel and then irradiated with NIR light, their viability decreased to just 32 % (Fig. 3B). Taken together, these results indicate that the DOPA-rGO@PC-gel can effectively induce a therapeutic effect upon NIR laser irradiation, triggering the death of breast cancer cells.

In another study, Tan *et al.* reported the development of a Methylcellulose injectable hydrogel loaded with IR820 (photothermal agent), whose photothermal effect (808 nm, 2.5 W/cm^2, 5 min) could decrease the viability of K7M2wt cells to approximately 56 % [50]. Costa *et al.* produced a Thiol-Maleimide crosslinked Chitosan-Hyaluronic acid hydrogel that was also loaded with DOPA-rGO (150 μg/mL) [38]. When irradiated with NIR light (808 nm, 1.7 W/cm^2, 10 min), the Chitosan-Hyaluronic acid hydrogel loaded with DOPA-rGO could reduce the viability of the MCF-7 cells to 59 % [38]. In this work, the phototherapeutic effect mediated by the DOPA-rGO@PC-gel (99.94 μg/mL of DOPA-rGO; 808 nm, 1.7 W/cm^2, 10 min) decreased the viability of the MCF-7 cells to just 32 %. In this way, the DOPA-rGO@PC-gel has a good potential for application in the photothermal therapy of breast cancer cells.

3.4. Evaluation of the antibacterial activity of the DOPA-rGO@PC-gel

The administration of injectable *in situ* forming hydrogels is generally a minimally invasive procedure [22]. However, it still carries a risk of infection at the injection site [22]. This concern is particularly significant for cancer patients, who are often more susceptible to infections due to their weakened immune system [51].

To evaluate the antibacterial activity of the DOPA-rGO@PC-gel, this formulation was placed in contact with gram-positive (*S. aureus*) and gram-negative (*E. coli*) bacteria (Fig. 4A). Afterwards, the viability of the bacteria was determined through the resazurin method [39]. The data showed that the DOPA-rGO@PC-gel could decrease the viability of *S. aureus* to just 24 % (Fig. 4B). Furthermore, this formulation also reduced the viability of *E. coli* to just 33 % (Fig. 4B). Such effects can be attributed to the presence of Chitosan in the DOPA-rGO@PC-gel and are in agreement with the good antibacterial capacity of the Chitosan-based hydrogels [35,52]. Collectively, these findings suggest that the DOPA-rGO@PC-gel may be a promising macroscale technology for future antimicrobial applications.

4. Conclusion

In this work, and for the first time, a dual-crosslinked injectable *in situ* forming Pluronic F127/Chitosan hydrogel incorporating DOPA-rGO was developed for application in cancer photothermal therapy. The produced hydrogels demonstrated an adequate injectability (through 21 G needles) and a good *in situ* gelation capacity. The dual-crosslinking present on the DOPA-rGO@PC-gel facilitated the formation of structures with interconnected pores and prevented the hydrogel's premature

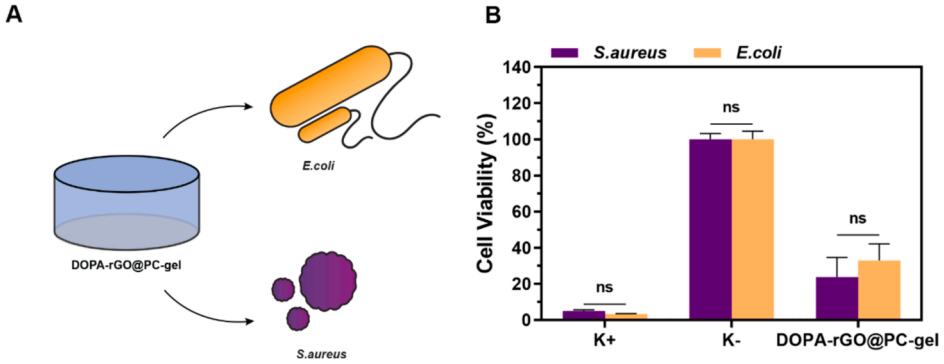

Fig. 4. Evaluation of the antibacterial activity mediated by the DOPA-rGO@PC-gel. Schematic illustration of the antibacterial assay (A). Analysis of the viability of *S. aureus* and *E. coli* after being exposed to the DOPA-rGO@PC-gel (B). Data represents mean ± S.D., n = 5 (n.s. = non-significant). K- and K+ represent the negative and positive controls, respectively.

degradation. The incorporation of the DOPA-rGO in the DOPA-rGO@PC-gel further improved the hydrogel's degradation profile. Upon exposure to NIR light, the DOPA-rGO@PC-gel produced a temperature increase of ≈ 22 °C (ΔT), which highlighted its robust photothermal capacity. The *in vitro* studies showed that the DOPA-rGO@PC-gel has a good cytocompatible profile towards both NHDF and MCF-7 cells (viability > 73 %). Importantly, the combined action of DOPA-rGO@PC-gel and NIR light decreased the viability of the MCF-7 cells to just 32 %, highlighting the excellent phototherapeutic capacity of this formulation. In addition, the DOPA-rGO@PC-gel exhibited a good antibacterial activity by reducing the viability of *S. aureus* and *E. coli* to 24 % and 33 %, respectively, which may be important to minimize the risk of infection at the injection site. Overall, the DOPA-rGO@PC-gel is a promising macroscale technology for breast cancer photothermal therapy and antimicrobial applications. In the future, *in vivo* studies will be crucial to confirm the DOPA-rGO@PC-gel's biodegradability/biocompatibility and phototherapeutic efficacy. Additionally, the antimicrobial properties of the DOPA-rGO@PC-gel may be further enhanced by incorporating additional agents (*e.g.*, curcumin, silver nanoparticles) in this formulation. Such may open a venue to explore this macroscale technology in the treatment of bacterial infections and/or wound healing applications.

CRediT authorship contribution statement

Manuel R. Pouso: Writing – original draft, Investigation, Formal analysis, Conceptualization. **Bruna L. Melo:** Investigation, Writing – review & editing. **Joaquim J. Gonçalves:** Writing – review & editing, Investigation. **António G. Mendonça:** Writing – review & editing, Supervision, Funding acquisition. **Ilídio J. Correia:** Funding acquisition, Project administration, Supervision, Writing – review & editing. **Duarte de Melo-Diogo:** Writing – review & editing, Supervision, Project administration, Funding acquisition, Conceptualization.

Declaration of Competing Interest

The authors declare that they have no known competing financial interests or personal relationships that could have appeared to influence the work reported in this paper.

Data availability

Data will be made available on request.

Acknowledgments

This work was developed within the scope of the CICS-UBI (Portugal) projects with the DOI 10.54499/UIDB/00709/2020 (https://doi.org/10.54499/UIDB/00709/2020) and DOI 10.54499/UIDP/00709/2020 (https://doi.org/10.54499/UIDP/00709/2020), supported by national funds through the Portuguese Foundation for Science and Technology/MCTES (Portugal). The funding from PTDC/BTABTA/0696/2020, 2022.06320.PTDC (DOI 10.54499/2022.06320.PTDC), 10.54499/LA/P/0079/2020 and 10.54499/UIDB/50022/2020 is also acknowledged. Duarte de Melo-Diogo acknowledges FCT for the financial support given through a Junior Researcher contract (2021.00590.CEECIND; DOI 10.54499/2021.00590.CEECIND/CP1661/CT0001). Manuel R. Pouso acknowledges a Research Fellowship funded by the project 2022.06320.PTDC (DOI 10.54499/2022.06320.PTDC). Bruna L. Melo acknowledges the funding from an individual PhD fellowship from FCT (2021.06044.BD).

Appendix A. Supplementary data

Supplementary data to this article can be found online at https://doi.org/10.1016/j.ejpb.2024.114476.

References

[1] M.J. Mitchell, M.M. Billingsley, R.M. Haley, M.E. Wechsler, N.A. Peppas, R. Langer, Engineering precision nanoparticles for drug delivery, Nat. Rev. Drug Discov. 20 (2021) 101–124.
[2] A.C. Anselmo, S. Mitragotri, Nanoparticles in the clinic: an update post COVID-19 vaccines, Bioeng. Transl. Med. 6 (2021) e10246.
[3] V. Pandey, T. Haider, A.R. Chandak, A. Chakraborty, S. Banerjee, V. Soni, Surface modified silk fibroin nanoparticles for improved delivery of doxorubicin: development, characterization, in-vitro studies, Int. J. Biol. Macromol. 164 (2020) 2018–2027.
[4] X. Wan, J.J. Beaudoin, N. Vinod, Y. Min, N. Makita, H. Bludau, R. Jordan, A. Wang, M. Sokolsky, A.V. Kabanov, Co-delivery of paclitaxel and cisplatin in poly(2-oxazoline) polymeric micelles: Implications for drug loading, release, pharmacokinetics and outcome of ovarian and breast cancer treatments, Biomaterials 192 (2019) 1–14.
[5] S. Khaledi, S. Jafari, S. Hamidi, O. Molavi, S. Davaran, Preparation and characterization of PLGA-PEG-PLGA polymeric nanoparticles for co-delivery of 5-Fluorouracil and Chrysin, J. Biomater. Sci. Polym. Ed. 31 (2020) 1107–1126.
[6] A. Manzari-Tavakoli, A. Babajani, M.M. Tavakoli, F. Safaeinejad, A. Jafari, Integrating natural compounds and nanoparticle-based drug delivery systems: a novel strategy for enhanced efficacy and selectivity in cancer therapy, Cancer Med. 13 (2024) e7010.
[7] D. Chen, X. Liu, X. Lu, J. Tian, Nanoparticle drug delivery systems for synergistic delivery of tumor therapy, Front. Pharmacol. 14 (2023) 1111991.
[8] J. Park, Y. Choi, H. Chang, W. Um, J.H. Ryu, I.C. Kwon, Alliance with EPR Effect: combined strategies to Improve the EPR Effect in the Tumor Microenvironment, Theranostics 9 (2019) 8073–8090.
[9] R.A. Ward, S. Fawell, N. Floc'h, V. Flemington, D. McKerrecher, P.D. Smith, Challenges and Opportunities in Cancer Drug Resistance, Chem. Rev. 121 (2021) 3297–3351.
[10] H. Xiao, Y. Zheng, L. Ma, L. Tian, Q. Sun, Clinically-Relevant ABC transporter for anti-cancer drug resistance, Front. Pharmacol. 12 (2021) 648407.
[11] Y. Xiong, Y. Rao, J. Hu, Z. Luo, C. Chen, Nanoparticle-Based Photothermal Therapy for Breast Cancer Noninvasive Treatment, Adv Mater, 2023, p. 2305140.
[12] D. de Melo-Diogo, C. Pais-Silva, D.R. Dias, A.F. Moreira, I.J. Correia, Strategies to improve cancer photothermal therapy mediated by nanomaterials, Adv. Healthc. Mater. 6 (2017) 2192–2640.
[13] C. Jang, J.H. Lee, A. Sahu, G. Tae, The synergistic effect of folate and RGD dual ligand of nanographene oxide on tumor targeting and photothermal therapy in vivo, Nanoscale 7 (2015) 18584–18594.
[14] P. Huang, P. Rong, J. Lin, W. Li, X. Yan, M.G. Zhang, L. Nie, G. Niu, J. Lu, W. Wang, X. Chen, Triphase interface synthesis of plasmonic gold bellflowers as near-infrared light mediated acoustic and thermal theranostics, J. Am. Chem. Soc. 136 (2014) 8307–8313.
[15] M. Chen, X. Fang, S. Tang, N. Zheng, Polypyrrole nanoparticles for high-performance in vivo near-infrared photothermal cancer therapy, Chem. Commun. (Camb) 48 (2012) 8934–8936.
[16] L.N.M. Nguyen, W. Ngo, Z.P. Lin, S. Sindhwani, P. MacMillan, S.M. Mladjenovic, W.C.W. Chan, The mechanisms of nanoparticle delivery to solid tumours, Nat. Rev. Bioeng. 2 (2024) 201–213.
[17] S. Wilhelm, A.J. Tavares, Q. Dai, S. Ohta, J. Audet, H.F. Dvorak, W.C.W. Chan, Analysis of nanoparticle delivery to tumours, Nat. Rev. Mater. 1 (2016).
[18] N.B. Alsaleh, J.M. Brown, Immune responses to engineered nanomaterials: current understanding and challenges, Curr Opin Toxicol 10 (2018) 8–14.
[19] Y. Li, G. Wang, L. Griffin, N.K. Banda, L.M. Saba, E.V. Groman, R. Scheinman, S. M. Moghimi, D. Simberg, Complement opsonization of nanoparticles: differences between humans and preclinical species, J. Control. Release 338 (2021) 548–556.
[20] A. Dhaliwal, G. Zheng, Improving accessibility of EPR-insensitive tumor phenotypes using EPR-adaptive strategies: designing a new perspective in nanomedicine delivery, Theranostics 9 (2019) 8091–8108.
[21] R. Sun, J. Xiang, Q. Zhou, Y. Piao, J. Tang, S. Shao, Z. Zhou, Y.H. Bae, Y. Shen, The tumor EPR effect for cancer drug delivery: current status, limitations, and alternatives, Adv. Drug Deliv. Rev. 191 (2022) 114614.
[22] R. Lima-Sousa, C.G. Alves, B.L. Melo, F.J.P. Costa, M. Nave, A.F. Moreira, A. G. Mendonca, I.J. Correia, D. de Melo-Diogo, Injectable hydrogels for the delivery of nanomaterials for cancer combinatorial photothermal therapy, Biomater. Sci. 11 (2023) 6082–6108.
[23] C.F. Martins, C. Garcia-Astrain, J. Conde, L.M. Liz-Marzan, Nanocomposite hydrogel microneedles: a theranostic toolbox for personalized medicine, Drug Deliv Transl Res 14 (2024) 2262–2274.
[24] X. Xu, Z. Huang, Z. Huang, X. Zhang, S. He, X. Sun, Y. Shen, M. Yan, C. Zhao, Injectable, NIR/pH-Responsive nanocomposite hydrogel as long-acting implant for chemophotothermal synergistic cancer therapy, ACS Appl. Mater. Interfaces 9 (2017) 20361–20375.
[25] C. Cheng, X. Zhang, Y. Meng, L. Chen, Q. Zhang, Development of a dual drug-loaded hydrogel delivery system for enhanced cancer therapy: in situ formation, degradation and synergistic antitumor efficiency, J. Mater. Chem. B 5 (2017) 8487–8497.
[26] Q. Zou, R. Chang, R. Xing, C. Yuan, X. Yan, Injectable self-assembled bola-dipeptide hydrogels for sustained photodynamic prodrug delivery and enhanced tumor therapy, J. Control. Release 319 (2020) 344–351.
[27] Y. Jiang, N. Krishnan, J. Heo, R.H. Fang, L. Zhang, Nanoparticle-hydrogel superstructures for biomedical applications, J. Control. Release 324 (2020) 505–521.

[28] P. Huang, H. Song, Y. Zhang, J. Liu, J. Zhang, W. Wang, J. Liu, C. Li, D. Kong, Bridging the Gap between Macroscale Drug Delivery systems and nanomedicines: a nanoparticle-assembled thermosensitive hydrogel for peritumoral chemotherapy, ACS Appl. Mater. Interfaces 8 (2016) 29323–29333.
[29] X. Zhou, X. He, K. Shi, L. Yuan, Y. Yang, Q. Liu, Y. Ming, C. Yi, Z. Qian, Injectable Thermosensitive Hydrogel Containing Erlotinib-loaded hollow mesoporous silica nanoparticles as a localized Drug delivery System for NSCLC Therapy, Adv Sci (weinh) 7 (2020) 2001442.
[30] J. Yu, H. Qiu, S. Yin, H. Wang, Y. Li, Polymeric drug delivery system based on pluronics for cancer treatment, Molecules 26 (2021) 3610.
[31] B. Li, L. Zhang, Z. Zhang, R. Gao, H. Li, Z. Dong, Q. Wang, Q. Zhou, Y. Wang, Physiologically stable F127-GO supramolecular hydrogel with sustained drug release characteristic for chemotherapy and photothermal therapy, RSC Adv. 8 (2018) 1693–1699.
[32] D.A. Won, M. Kim, G. Tae, Systemic modulation of the stability of pluronic hydrogel by a small amount of graphene oxide, Colloids Surf. B Biointerfaces 128 (2015) 515–521.
[33] H. Carrêlo, A.R. Escoval, P.I.P. Soares, J.P. Borges, M.T. Cidade, Injectable Composite Systems of Gellan Gum: Alginate microparticles in pluronic hydrogels for bioactive cargo controlled Delivery: optimization of hydrogel composition based on rheological behavior, Fluids 7 (2022) 375.
[34] J. Garcia-Couce, M. Tomas, G. Fuentes, I. Que, A. Almirall, L.J. Cruz, Chitosan/Pluronic F127 Thermosensitive Hydrogel as an Injectable Dexamethasone Delivery Carrier, Gels 8 (2022) 44.
[35] R. Lima-Sousa, D. de Melo-Diogo, C.G. Alves, C.S.D. Cabral, S.P. Miguel, A. G. Mendonca, I.J. Correia, Injectable in situ forming thermo-responsive graphene based hydrogels for cancer chemo-photothermal therapy and NIR light-enhanced antibacterial applications, Mater Sci Eng C Mater Biol Appl 117 (2020) 111294.
[36] R. Lima-Sousa, C.G. Alves, B.L. Melo, A.F. Moreira, A.G. Mendonca, I.J. Correia, D. de Melo-Diogo, Poly(2-ethyl-2-oxazoline) functionalized reduced graphene oxide: optimization of the reduction process using dopamine and application in cancer photothermal therapy, Mater Sci Eng C Mater Biol Appl 130 (2021) 112468.
[37] B.L. Melo, R. Lima-Sousa, C.G. Alves, A.F. Moreira, I.J. Correia, D. de Melo-Diogo, Chitosan-based injectable in situ forming hydrogels containing dopamine-reduced graphene oxide and resveratrol for breast cancer chemo-photothermal therapy, Biochem. Eng. J. 185 (2022) 108529.
[38] F.J.P. Costa, M. Nave, R. Lima-Sousa, C.G. Alves, B.L. Melo, I.J. Correia, D. de Melo-Diogo, Development of Thiol-Maleimide hydrogels incorporating graphene-based nanomaterials for cancer chemo-photothermal therapy, Int. J. Pharm. 635 (2023) 122713.
[39] S.P. Miguel, M.P. Ribeiro, H. Brancal, P. Coutinho, I.J. Correia, Thermoresponsive chitosan-agarose hydrogel for skin regeneration, Carbohydr. Polym. 111 (2014) 366–373.
[40] B. Liu, K. Chen, Advances in Hydrogel-Based Drug Delivery Systems, Gels 10 (2024) 262.
[41] K.J. Rambhia, P.X. Ma, Controlled drug release for tissue engineering, J. Control. Release 219 (2015) 119–128.
[42] J. Li, E. Weber, S. Guth-Gundel, M. Schuleit, A. Kuttler, C. Halleux, N. Accart, A. Doelemeyer, A. Basler, B. Tigani, K. Wuersch, M. Fornaro, M. Kneissel, A. Stafford, B.R. Freedman, D.J. Mooney, Tough Composite Hydrogels with High Loading and Local Release of Biological Drugs, Adv. Healthc. Mater. 7 (2018) 1701393.
[43] Y. Hao, Y. Liu, Y. Wu, N. Tao, D. Lou, J. Li, X. Sun, Y.N. Liu, A robust hybrid nanozyme@hydrogel platform as a biomimetic cascade bioreactor for combination antitumor therapy, Biomater. Sci. 8 (2020) 1830–1839.
[44] K.K. Lee, S.C. Lee, H. Kim, C.-S. Lee, Polydopamine Nanoparticle-Incorporated Fluorescent Hydrogel for Fluorescence Imaging-Guided Photothermal Therapy of Cancers, BioChip J. 17 (2022) 85–92.
[45] H. Chen, Y. Ma, X. Wang, Z. Zha, Multifunctional phase-change hollow mesoporous Prussian blue nanoparticles as a NIR light responsive drug co-delivery system to overcome cancer therapeutic resistance, J. Mater. Chem. B 5 (2017) 7051–7058.
[46] L. Sun, Z. Li, Z. Li, Y. Hu, C. Chen, C. Yang, B. Du, Y. Sun, F. Besenbacher, M. Yu, Design and mechanism of core-shell TiO(2) nanoparticles as a high-performance photothermal agent, Nanoscale 9 (2017) 16183–16192.
[47] Y. Liang, M. Wang, Z. Zhang, G. Ren, Y. Liu, S. Wu, J. Shen, Facile synthesis of ZnO QDs@GO-CS hydrogel for synergetic antibacterial applications and enhanced wound healing, Chem. Eng. J. 378 (2019) 122043.
[48] C. Yu, L. Li, D. Liang, A. Wu, Q. Dong, S. Jia, Y. Li, Y. Li, X. Guo, H. Zang, Glycosaminoglycan-based injectable hydrogels with multi-functions in the alleviation of osteoarthritis, Carbohydr. Polym. 290 (2022) 119492.
[49] I.J. Sabino, R. Lima-Sousa, C.G. Alves, B.L. Melo, A.F. Moreira, I.J. Correia, D. de Melo-Diogo, Injectable in situ forming hydrogels incorporating dual-nanoparticles for chemo-photothermal therapy of breast cancer cells, Int. J. Pharm. 600 (2021) 120510.
[50] B. Tan, Y. Wu, Y. Wu, K. Shi, R. Han, Y. Li, Z. Qian, J. Liao, Curcumin-Microsphere/IR820 Hybrid Bifunctional Hydrogels for In Situ Osteosarcoma Chemo-co-Thermal Therapy and Bone Reconstruction, ACS Appl. Mater. Interfaces 13 (2021) 31542–31553.
[51] J. Wang, X. Wu, P. Shen, J. Wang, Y. Shen, Y. Shen, T.J. Webster, J. Deng, Applications of Inorganic Nanomaterials in Photothermal Therapy Based on Combinational Cancer Treatment, Int. J. Nanomed. 15 (2020) 1903–1914.
[52] P. Deng, L. Yao, J. Chen, Z. Tang, J. Zhou, Chitosan-based hydrogels with injectable, self-healing and antibacterial properties for wound healing, Carbohydr. Polym. 276 (2022) 118718.